Computing Charging and Polarization Energies of Small Organic Molecules Embedded into Amorphous Materials with Quantum Accuracy

Jonas Armleder, Timo Strunk, Franz Symalla, Pascal Friederich, Jorge Enrique Olivares Peña, Tobias Neumann, Wolfgang Wenzel, and Artem Fediai*

ABSTRACT: The ionization potential, electron affinity, and cation/anion polarization energies (IP, EA, $P^{(+)}$, $P^{(-)}$) of organic molecules determine injection barriers, charge carriers balance, doping efficiency, and light outcoupling in organic electronics devices, such as organic light emitting diodes (OLEDs). Computing IP and EA of isolated molecules is a common task for quantum chemistry methods. However, once molecules are embedded in an amorphous organic matrix, IP and EA values change, and accurate predictions become challenging. Here, we present a revised quantum embedding method [Friederich et al. *J. Chem. Theory Comput.* **2014**, *10* (9), 3720−3725] that accurately predicts the dielectric permittivity and ionization potentials in three test materials, NPB, TCTA, and C60, and allows straightforward interpretation of their nature. The method paves the way toward reliable virtual screening of amorphous organic semiconductors with targeted IP/EA, polarization energies, and relative dielectric permittivity.

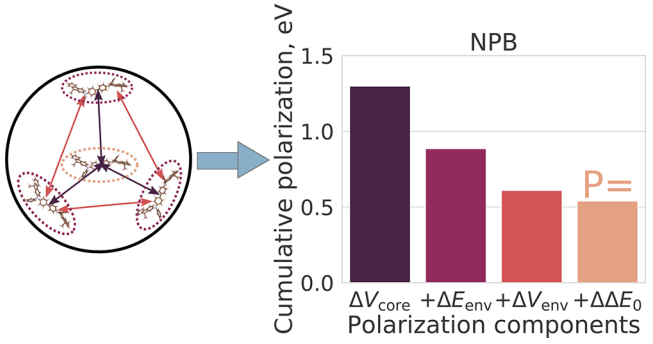

1. INTRODUCTION

Organic semiconductors (OS) are materials used in organic light emitting diodes (OLEDs),[1] organic field effect transistors,[2] organic solar cells,[3] and other already commercialized or promising technologies. Due to the large chemical space accessible by synthetic organic chemistry, many properties of organic molecules may, in principle, be tuned to satisfy particular requirements.[4] Organic semiconductors inherit properties of constituent molecules to a certain extent. However, due to molecule specific intermolecular interactions in thin films, explicit models of these environmental effects are required to translate molecular properties to the material or device level.[5−7] It is well known that due to a weak electrostatic screening (ϵ_r = 2, ...,5) and charge localization, the ionization potential (IP) and electron affinity (EA) of the organic molecules in a matrix differ from their vacuum counterparts by a magnitude that may exceed 2 eV.[5] Moreover, the host dependent variation of dopant's IP/EA can exceed 1 eV, and an accurate description of these polarization effects is crucial for the design of efficient dopants and emitters.[6,8−12]

OLEDs still suffer from a short lifetime or low efficiency especially for blue emitters. These challenges are tackled with setups of increasing complexity, e.g., emission systems combining multiple materials in a single layer. Identification of materials with only experimental methods is time consuming and costly. A virtual design can support experimental efforts with efficient and accurate computation of the polarization, IP, and EA of the embedded organic molecules. Several methods have been proposed to theoretically describe the polarization response of the environment and the intermolecular interactions.[5] In the polarizable force field methods (PFF), molecular polarization response is parametrized either by atomic polarizabilities or a charge response tensor.[13−16] In approaches combining quantum mechanics (QM) and molecular mechanics (MM), particular molecules are treated on a quantum mechanical level, and their polarizable environment is treated on a classical level.[17−21] The necessity to parametrize the force fields limits their accuracy and prevents full virtual design. Furthermore, the parametrization often requires experimental data. The full quantum mechanical approaches, valence bond Hartree−Fock (VBHF),[22,23] and constrained density functional theory (CDFT)[24] overcome this problem by employing Hartree−Fock or density functional theory (DFT) for the molecular

polarization response, but they are computationally very demanding. Besides, these methods need artificial potentials to confine charge carriers to certain molecules, limiting their accuracy. Finally, the mentioned methods are mostly applicable to crystalline organic semiconductors, while state of the art OLEDs consist of amorphous organic semiconductors.

In this work, we overcome these limitations by treating intramolecular interactions in organic thin film at a QM level (DFT or GW) while describing intermolecular interactions in terms of partial charges derived from QM simulations. Our approach extends and improves the so called Quantum Patch method[7,25] which is a subclass of subsystem DFT.[26−28] In subsystem DFT, the electron density is split into subsystem densities whose energy is minimized in an embedding potential of the other subsystems. The embedding potential is composed of an electrostatic part and contributions arising from the kinetic potential and the exchange correlation. In the Quantum Patch method, these subsystems are represented by molecules that only interact with each other via electrostatic interaction, while intermolecular exchange correlation is neglected—a reasonable assumption for molecules in amorphous OS which are separated by van der Waals distances. The Quantum Patch method enables linear scaling of computational effort with the number of molecules. This work extends the method as follows: (1) In addition to the polarization response of environmental molecules (the polarization itself), an internal contribution and environmental depolarization effects are taken into account, decreasing the polarization energy. (2) The polarization energy is extrapolated to its bulk value which incorporates the polarization energy outside the explicitly atomistic simulated region. In fact, this is equal to computing the polarization energy of the outer region at a level of classical electrostatics with the dielectric permittivity extracted from the explicit simulation. Furthermore, our approach modifies the original method by using different techniques, GW and DFT, to compute the energy of the molecule of interest and the polarization of the environmental molecules, respectively. The method is an efficient tool to support experimental research and development to overcome persisting OLED and OPV design challenges.

The paper is organized as follows. Section 2 describes the underlying formalism and the method to extract IP, EA, polarization energies, and dielectric permittivity. In Section 3, the method is applied to predict properties of prototypical small molecule organic semiconductors used in OLEDs, *N*,*N*′ di(1 naphthyl) *N*,*N*′ diphenyl (1,1′ biphenyl) 4,4′ diamine (NPB), buckminsterfullerene (C_{60}), and 4,4′,4″ tris(carbazol 9 yl)triphenylamine (TCTA). Theoretical accuracy is estimated based on the accuracy of underlying methods, and the simulation results are compared to experimental data. Section 3 is followed by the Conclusion.

2. METHOD

2.1. Explicit Contributions to the Polarization Energy.

The ionization potential (IP) and electron affinity (EA) of an embedded molecule are defined as

$$\mathrm{IP} = E^{(+)} - E^{(0)} \tag{1}$$

$$\mathrm{EA} = E^{(0)} - E^{(-)} \tag{2}$$

where $E^{(0)}$, $E^{(+)}$, and $E^{(-)}$ are the total energy of the material with a specific molecule (hereinafter, the core molecule) in its neutral, cationic, and anionic states, respectively.

Embedded molecule IP and EA differ from those in a vacuum, IP(vac) and EA(vac), by the quantities called cation/anion polarization energies, $\mathrm{P}^{(+)}$ and $\mathrm{P}^{(-)}$, respectively. These are defined as

$$\mathrm{P}^{(+)} = \mathrm{IP(vac)} - \mathrm{IP} \tag{3}$$

$$\mathrm{P}^{(-)} = \mathrm{EA} - \mathrm{EA(vac)} \tag{4}$$

where $\mathrm{IP(vac)} = E_0^{(+)}(\mathrm{vac}) - E_0^{(0)}(\mathrm{vac})$ and $\mathrm{EA(vac)} = E_0^{(0)}(\mathrm{vac}) - E_0^{(-)}(\mathrm{vac})$, where $E_0^{(\pm/0)}(\mathrm{vac})$ is the energy of the cation/anion/neutral core molecule in vacuum.

The original Quantum Patch method[7,25] and its extension presented here are designed for disordered organic semiconductors, i.e., nonperiodic solids. Therefore, the treatment of the infinite system by going into reciprocal space is impossible. Instead, we compute a part of the material within a finite radius R_{cut} explicitly. The contribution to the polarization energy of the remaining polarizable environment ($r > R_{\mathrm{cut}}$) that was ignored in the original Quantum Patch method[7] is taken into account implicitly in this work, see Section 2.2.

Figure 1 shows a core molecule in its neutral and charged (cationic) state inside the explicit polarization shell. Systems

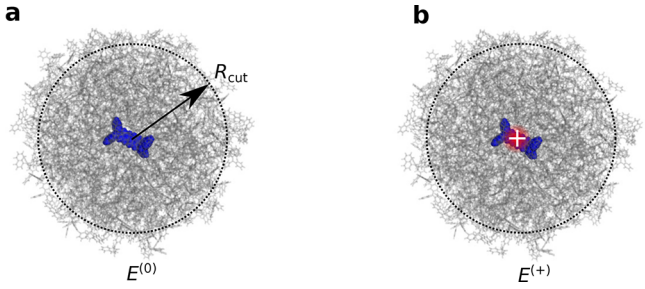

Figure 1. Two molecular systems are explicitly simulated to determine the ionization potential of the embedded molecule: (a) neutral molecule (shown in blue) embedded into the material inside the sphere with R_{cut} radius and (b) same as (a) with a positively charged core molecule. Both systems are meant to be electronically equilibrated. The ionization potential, IP, of the embedded molecule is computed by definition, i.e., $\mathrm{IP} = E^{(+)} - E^{(0)}$, where $E^{(+)}$ and $E^{(0)}$ contain energy contributions from the explicit shell and the outer region.

(a) and (b) are meant to be electronically equilibrated to compute the ionization potential (IP).

The energy of the interacting molecular system within a sphere with radius $R < R_{\mathrm{cut}}$ is denoted as $E^{(\pm/0)}(R)$. It is divided into two contributions: The energies of individual molecules, $E_i^{(\pm/0)}$, where i is the index of the molecule, which is computed at the DFT level. These energies differ from the energy the molecule would have in vacuum and the energy of intermolecular interactions, $V_{ij}^{(\pm/0)}$, computed via Coulomb interaction of electrostatic potential (ESP) partial charges of a molecular pair i and j, with densities $n_i^{\mathrm{pcs}}(\mathbf{r})$ and $n_j^{\mathrm{pcs}}(\mathbf{r})$, respectively. i and j iterate only over molecules within the sphere with radius R. The superscript (+/− /0) denotes the charged state of the core molecule (cation/anion/neutral):

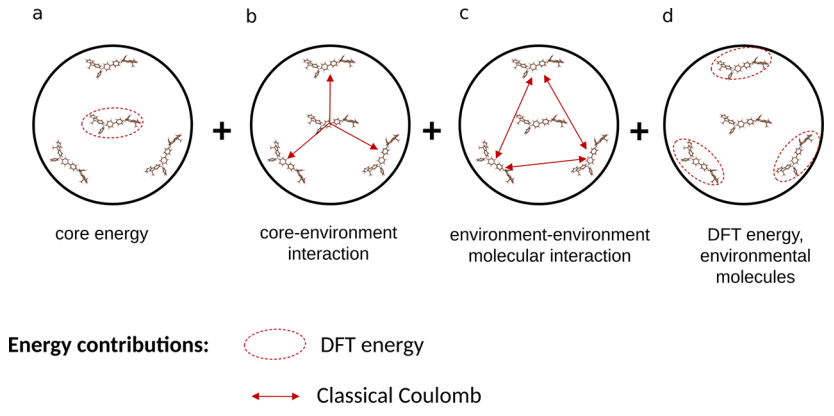

Figure 2. Components of the total energy $E^{(\pm/0)}$ of the material: (a) the energy of the core molecule (DFT level), (b) core environment Coulomb interaction energy, (c) Coulomb interaction between environmental molecules, and (d) internal (DFT) energy of environmental molecules. The original Quantum Patch method[7] took only (a) and (b) components into account significantly overestimating the polarization energy.

$$E^{(+/-/0)}(R) = \sum_{i=0}^{N} E_i^{(+/-/0)} + \sum_{i=0}^{N}\sum_{j>i}^{N} V_{ij}^{(+/-/0)} \tag{5}$$

To get the full energy of the system, $E^{(\pm/0)}(R)$ has to be corrected by the energy outside the sphere. The explicit definition of V_{ij} is as follows (in au):

$$V_{ij} = \int\int \frac{n_i^{\mathrm{pcs}}(\mathbf{r}) n_j^{\mathrm{pcs}}(\mathbf{r}')}{|\mathbf{r} - \mathbf{r}'|}\, \mathrm{d}\mathbf{r}\, \mathrm{d}\mathbf{r}' \tag{6}$$

In the Quantum Patch method, the DFT density of every ith molecule is computed self consistently in the field of partial charges of all other molecules ($j \in \{0,1,...,N\}\backslash i$). It includes the $N + 1$ *inner* self consistent field (SCF) loops—DFT simulations of every molecule in a field of point charges due to all other molecules. During the inner SCF loop, the ESP partial charges of surrounding molecules do not change. As all $N + 1$ simulations of the inner loop are done, the next step of the *outer* SCF loop is performed where the partial charges are updated based on new DFT densities. The outer loop has finished when the total energy of the explicitly simulated system is converged. To determine IP/EA, this procedure is performed once for the neutral and once for the positively/negatively charged core molecule. The constraint of the charged state of the core molecule is not required because only one molecule is quantum mechanically simulated at a time. In contrast, from the point of view of this specific molecule, all other molecules are only sources of the electrical field. Figure S1 in the Supporting Information illustrates the method. Figure 2 shows energy contributions to the material energy, split according to the level of theory used to estimate them (DFT or classical interactions of DFT derived partial charges). The first two contributions (a) and (b) are already given in the original Quantum Patch method. The main difference of this work and the previous work is adding the contributions (c) (Coulomb interaction between environmental molecules) and (d) (internal (DFT) energy of environmental molecules). Furthermore, this leads to a new convergence criterion, which requires the total energy of the system, $E^{(\pm/0)}$, to converge rather than its part, the Coulomb interaction energy between the core and environmental molecules, $\sum_j^N {}_0 V_{0j}$. This doubles the number of required interactions (steps) of the outer loop.

While the method takes exchange correlation interactions only intramolecularly into account, intermolecularly they are neglected. The latter assumption is well justified for amorphous organic semiconductors, as their molecules are separated by van der Waals distances leading to a small intermolecular overlap of orbitals. Additionally, it is assumed that ESP partial charges accurately reproduce the electric field generated by a molecule at relevant distances. An exemplary calculation for C60 shows that at distances larger than 7 Å, ESP partial charges accurately reproduce the potential created by the actual (DFT) charge density, see Supporting Information, Figure S2. It is convenient to split the energy difference in eq 1 into four components according to their nature (see Figure 2)

$$\mathrm{IP}(R) = \Delta E_0^{(+)} - \Delta V_0^{(+)}(R) - \Delta V_{\mathrm{env}}^{(+)}(R) - \Delta E_{\mathrm{env}}^{(+)}(R) \tag{7}$$

where

$$\Delta E_0^{(+)} = E_0^{(+)} - E_0^{(0)}$$

is the difference in DFT energies of the core molecule in its different charged states,

$$\Delta V_0^{(+)}(R) = \sum_{i=1}^{N} [V_{0i}^{(0)} - V_{0i}^{(+)}]$$

is the difference in Coulomb interactions of the core molecule with all environmental molecules,

$$\Delta V_{\mathrm{env}}^{(+)}(R) = \sum_{i=1}^{N}\sum_{j>i}^{N} [V_{ij}^{(0)} - V_{ij}^{(+)}]$$

is the difference in total interaction energies of all environmental molecules, and

$$\Delta E_{\mathrm{env}}^{(+)}(R) = \sum_{i=1}^{N} [E_i^{(0)} - E_i^{(+)}]$$

is the difference in DFT internal energies of all environmental molecules.

The cation polarization energy $\mathrm{P}^{(+)}$ expressed element wise reads

$$\mathrm{P}^{(+)}(R) = \Delta\Delta E_0^{(+)} + \Delta V_0^{(+)}(R) + \Delta V_{\mathrm{env}}^{(+)}(R) + \Delta E_{\mathrm{env}}^{(+)}(R) \tag{8}$$

with

$$\Delta\Delta E_0^{(+)} = -[E_0^{(+)} - E_0^{(+)}(\mathrm{vac})] + [E_0^{(0)} - E_0^{(0)}(\mathrm{vac})] \tag{9}$$

The anion polarization energy, $\mathrm{P}^{(-)}$, can be expressed similarly

$$\mathrm{P}^{(-)}(R) = \Delta\Delta E_0^{(-)} + \Delta V_0^{(-)}(R) + \Delta V_{\mathrm{env}}^{(-)}(R) + \Delta E_{\mathrm{env}}^{(-)}(R) \tag{10}$$

where the four terms on the right hand side are defined analogously to those of $\mathrm{P}^{(+)}(R)$ (eq 8). Eq 9 can be rewritten as

$$\Delta\Delta E_0^{(+)} = \mathrm{IP}(\mathrm{vac}) - \Delta E_0^{(+)} \tag{11}$$

where $\Delta E_0^{(+)}$ has the sense of the ionization potential of the embedded molecule, provided that its electron density was self consistently determined in the polarizable environment ("equilibrated"). Still, the interaction with the environment is set to zero ("damped") after such "equilibration". It is thus close but not equivalent to the IP of a molecule in a vacuum.

2.2. Implicit Part of the Polarization Energy and the Dielectric Permittivity. The method described above explicitly computes $\mathrm{P}^{(+)}/\mathrm{P}^{(-)}$/IP/EA of a core molecule embedded into a finite molecular cluster of radius R_{cut} (see Figure 1): $P_{\mathrm{expl}} = \mathrm{P}(r < R_{\mathrm{cut}})$. The rest of the polarization energy, $P_{\mathrm{impl}} = P(r > R_{\mathrm{cut}})$, is approximated by the polarization energy of the continuous medium with dielectric permittivity ϵ_r, computed from the classical electrostatics:[29]

$$\mathrm{P}_{\mathrm{impl}} = (1 - 1/\epsilon_r)\frac{e^2}{8\epsilon_0\pi R_{\mathrm{cut}}} \tag{12}$$

Here, e and ϵ_0 are the elementary charge and the vacuum permittivity. The bulk polarization energy is therefore

$$\mathrm{P}^{(+/-)} = \mathrm{P}_{\mathrm{expl}}^{(+/-)} + \mathrm{P}_{\mathrm{impl}}^{(+/-)} \tag{13}$$

In practice, the dielectric permittivity can be determined if we look at eq 12 from a different perspective. For large R_{cut} (where quantum and classical description approximately coincide), $\mathrm{P}^{(\pm)}$ does not depend on the chosen R_{cut}. Thus, we can consider the R_{cut} as a variable, R, leading to an expression

$$\mathrm{P}^{(+/-)} = \mathrm{P}_{\mathrm{expl}}^{(+/-)}(R) + (1 - 1/\epsilon_r)\frac{e^2}{8\epsilon_0\pi R} \tag{14}$$

Differentiating eq 14 with respect to $1/R$ allows establishing a relation between the dielectric permittivity ϵ_r and the slope of the dependence $\mathrm{P}_{\mathrm{expl}}^{(\pm)}(1/R)$

$$\epsilon_r = -\frac{c}{c - \mathrm{slope}} \tag{15}$$

where $c \equiv e^2/(8\pi\epsilon_0)$ is a constant; $\mathrm{slope} \equiv \frac{\partial \mathrm{P}_{\mathrm{expl}}^{(+/-)}(1/R)}{\partial(1/R)} = \frac{\partial \mathrm{P}^{(+/-)}(1/R)}{\partial(1/R)}$ for $R < R_{\mathrm{cut}}$. Although the polarization energy is evaluated inside the polarization spheres with variable radii R up to R_{cut}, a self consistent field simulation (the electron density equilibration) is performed only once: for the polarization sphere of the radius R_{cut} that is for the whole explicit polarization shell. At large R, the polarization energy slope must be the same for anions and cations (because the classical theory of the polarization holds). To increase practical accuracy, we compute the dielectric permittivity from the explicit polarization energy slope averaged over cation and anion polarization: $\mathrm{P}^{(+/-)}(R) \rightarrow \mathrm{P}(R) \equiv \frac{1}{2}(\mathrm{P}^{(+)}(R) + \mathrm{P}^{(-)}(R))$. The reason for improved accuracy is that the polarizing part $\Delta V_0^{(\pm)}(R)$ of the polarization energy $\mathrm{P}^{(+/-)}(R)$ can be divided into two contributions: induced and static interaction energy. The induced interaction energy emerges from the induced dipole interaction of environment molecules with the charged core molecule, and the latter is the interaction between the molecular static dipoles and the charged core molecule; for a qualitative description, both contributions can be described as a dipole−monopole interaction. The induced dipoles will be aligned parallel to the electric field created by the additional charge of the core molecule. This causes the induced interaction energy to be approximately equal for a positive or negative charge of the core molecule. In contrast, the sign of the static interaction energy depends on the sign of the charge of the core molecule which means averaging over $\mathrm{P}^{(+/-)}(R)$ offsets the static interaction energy. The static interaction contribution is only significant for close by close molecules as far away molecules show only a small dipole−monopole interaction, and other molecules with the same distance will compensate their effect, as the orientation of static dipoles is randomly distributed. An alternative possibility to compute the slope $\frac{\partial \mathrm{P}^{(+/-)}(1/R)}{\partial(1/R)}$ is simulating very large explicit shells and extracting its value directly from $\mathrm{P}^{(+/-)}(R)$ which would be computationally very expensive and is hence not pursued.

As the internal (de)polarization contribution $\Delta\Delta E_0^{(+/-)}$ does not depend on R, we introduce the environmental polarization energy

$$\mathrm{P}_{\mathrm{env}}^{(+/-)}(R) \equiv \Delta V_0^{(+/-)}(R) + \Delta E_{\mathrm{env}}^{(+/-)}(R) + \Delta V_{\mathrm{env}}^{(+/-)}(R) \tag{16}$$

to compute the slope.

We note that the radial distribution function fluctuates considerably inside the explicit polarization sphere. This leads to the fluctuation of the extracted dielectric permittivity depending on the interval chosen to compute the slope. Therefore, we introduce the so called renormalized radius $\tilde{R}$, which is related to the number of molecules inside a given polarization radius, which leads to a smoothed material density

$$\tilde{R} = \left[\frac{3}{4\pi}N(R)/n\right]^{1/3} \tag{17}$$

where $N(R)$ is the number of molecules, which centers of geometries (COGs) are inside the radius R, and n is the number density of the material. The relation between R and $\tilde{R}$ is provided in Supporting Information, Figure S3.

3. RESULTS

3.1. The Validation Set of Materials. Three prototypical small molecules organic semiconductors, C60, NPB, and TCTA, were simulated to make a preliminary model validation. Materials morphology has been generated with the method DEPOSIT,[32] a Monte Carlo protocol that mimics the physical vapor deposition process and generates a morphology. The force field parameters used in DEPOSIT were computed by optimizing the geometry of a molecule using the def2 SV(P) basis set and B3LYP functional.[33] NPB and TCTA have been additionally parametrized for different dihedral configurations. One hundred sampling points per dihedral are simulated using the def2 SV(P) basis set and BP86[34] exchange correlation functional. In the course of simulations, the temperature was decreased from 4000 to

300 K. Sixty simulated annealing cycles, each with 50000 Monte Carlo steps, were performed for every molecule. In total, 2800 molecules were deposited for each material; their centers of geometries are within a 90 Å × 90 Å square. Periodic boundary conditions allow adding periodic copies in the x and y directions to obtain a base area of about 270 Å × 270 Å. Table 1 shows the size and the density of virtually deposited materials along with the experimental value of the materials' density. Deviations from the experimental density do not exceed 1.2%. The radial distribution function of materials is shown in Supporting Information, Figures S4–S6.

Table 1. Properties of the Deposited Pure Morphologies and the Comparison with Experimental Data[a]

molecule	morphology size, nm	comp. density, $\frac{g}{cm^3}$	exp. density, $\frac{g}{cm^3}$
NPB	28.8 × 28.8 × 30.3	1.133	1.14[30]
C60	27.7 × 27.7 × 24.4	1.707	1.72[31]
TCTA	28.9 × 28.7 × 38.1	1.127	1.14[30]

[a]The deviations from the experimental density do not exceed 1.2%.

3.2. Asymptotic Behavior of the Polarization Energy and Dielectric Permittivity. Figure 3a shows the environmental polarization radius dependent part of the polarization energy $P \equiv \frac{1}{2}(P_{env}^{(+)} + P_{env}^{(-)})$ as a function of the inverse renormalized polarization radius, $\tilde{R}$, averaged over five randomly selected core molecules from the depth of the simulated material. P_{env} is defined in eq 16 and lacks in comparison to the total polarization energy of the internal contribution $\Delta\Delta E_0^{(\pm)}$.

The radius of the explicit polarization sphere R_{cut} is 50 Å (i.e., all molecules, whose centers of geometry are inside the 50 Å sphere, are explicitly simulated). Black lines are least squares approximations of the dependence $P_{env}(1/\tilde{R})$ for points in the interval between 20 Å and 40 Å. The lower limit of the interval is chosen to avoid regions with a rapidly changing radial distribution function and near field effects. The upper limit is 10 Å smaller than R_{cut}; this is done to avoid noncorrectable boundary effects. Noticeable boundary effects, however, originate from the missing polarizable medium outside the explicit shell. The polarization energy $P_{env}^{(+)}$ shows sublinear behavior, and the $P_{env}^{(-)}$ superlinear behavior in $\frac{1}{R}$ is close to the cutoff radius, as plotted for NPB in the Supplementary Information, Figure S9. The missing dipoles from molecules with $R > R_{cut}$ influence the cation/anion polarization energy $P_{env}^{(+/-)}(R)$ in an opposite way. Formally, this can be described by $P_{env}^{(+/-)}(R)$ = environmental polarization energy $\mp$ non physical boundary contribution. Averaging over $P_{env}^{(+/-)}$ yields the environmental polarization energy P_{env} without finite size effects. An affirmation can be seen in Figure S9, and the average polarization energy P_{env} follows the linear trend predicted by the theory of macroscopic polarization. Line slopes are determined and inserted into eq 15 to obtain dielectric permittivity, ϵ_r. In Figure 3b, these values are plotted together with experimental values of dielectric permittivity taken from ref 37 (NPB), ref 35 (C60), and ref 36 (TCTA). The measurements do not include vibrational modes because the ellipsometry measurements provide only data for energies over 1–2 eV. This, in turn, implies that the measured $\epsilon_{r,opt}$ contains optically excited electronic modes. Our simulation can only predict the electrostatic value $\epsilon_{r,\infty}$ without vibrational and optically excited electronic modes. The experimental value $\epsilon_{r,\infty}$ is obtained from extrapolating $\epsilon_{r,opt}$ to infinite wavelengths $\lambda \to \infty$. Generally, this is expressed by the formula $\epsilon_{r,\infty} = \epsilon_{r,opt} - \delta$, where δ is the shift due to optically excited modes and is generally 0.05–0.15.[38] For NPB and TCTA, $\epsilon_{r,opt}$ was extrapolated to infinite wavelength; the value for C60 is already given as an extrapolated value.

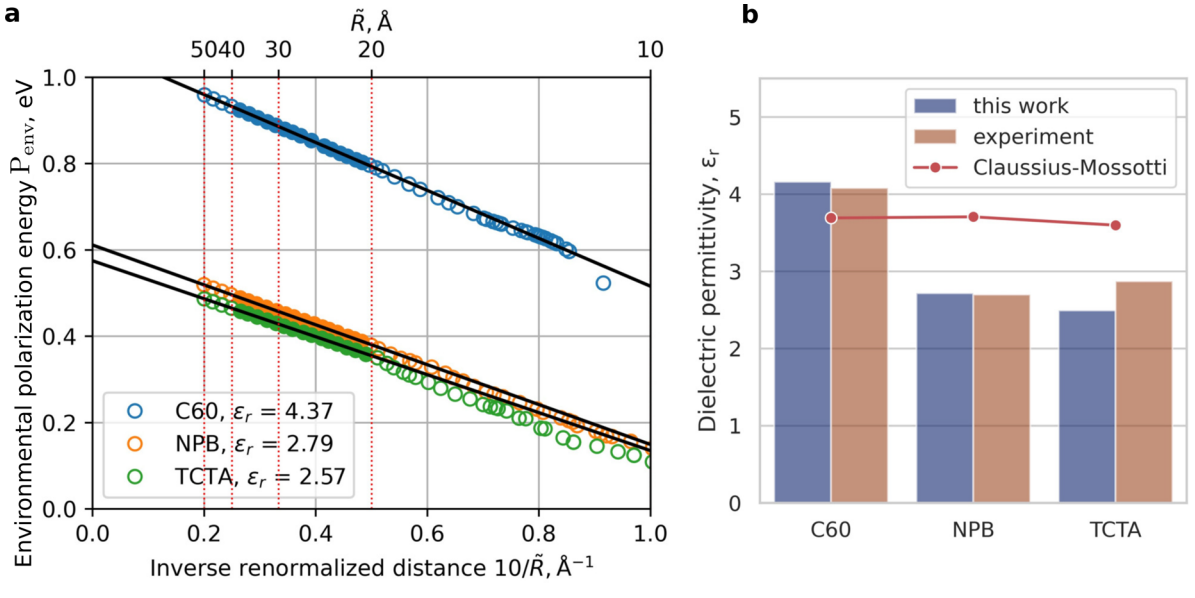

Figure 3. Extraction of the relative dielectric permittivity from the simulations. (a) Environmental polarization energy averaged over cation and anion, P_{env}, as a function of the renormalized radius $\tilde{R}$. The filled markers are used to obtain approximating lines (shown in black) and consequently compute the relative dielectric permittivity from their slopes (eq 15). (b) Comparing the relative dielectric permittivity ϵ_r computed in this work to that determined experimentally,[35–37] and calculated using the Clausius–Mossotti (CM) relation (eq 18). Our method predicts the trend of experimentally observed ϵ_r: ϵ_r of C60 is much larger than that of NPB or TCTA, while predictions based on the CM relation are highly inaccurate, both in terms of absolute values and the trend.

While our model predicts significantly higher dielectric permittivity of C60 and almost the same permittivity for TCTA and NPB, the Clausius−Mossotti (CM) relation[39]

$$\epsilon_r = \frac{3N_A\alpha\rho}{3M\epsilon_0 - N_A\alpha\rho} + 1 \tag{18}$$

does not distinguish among TCTA, NPB, and C60 demonstrating the necessity of using explicit atomistic models even for finding the macroscopic material parameter. In eq 18, N_A denotes the Avogadro constant, α is the mean molecular polarizability, ρ is the material density, M is the molar mass, and ϵ_0 is the vacuum permittivity. The polarizability tensor was computed with single point DFT as implemented in Turbomole[40] using the BP86[34] exchange correlation functional and def2 TZVPDD basis set; α is equal to 1/3 trace of the polarizability tensor by the above definition. The experimental values of the density from Table 1 were used as ρ. Table 2 summarizes experimental and computed values of $\epsilon_{r,\infty}$.

Table 2. Dielectric Permittivity Computed in This Work (ϵ_{sim}), Calculated via the Clausius−Mossotti Relation (ϵ_{CM}), and Determined Experimentally[35−37]

molecule	ϵ_{sim} (this work)	ϵ_{exp}	ϵ_{CM}
C60	4.2 ± 0.1	4.08[35]	3.69
NPB	2.72 ± 0.06	2.7[37]	3.71
TCTA	2.49 ± 0.05	2.87[36]	3.60

3.3. Components of the Polarization Energy. Figure 4a shows various components of the environmental polarization energy P_{env} as a function of the polarization radius for C60. $P_{env}(R)$ is averaged over the cationic ($P^{(+)}_{env}(R)$) and the anionic ($P^{(-)}_{env}(R)$) values for five core molecules. Dependencies for NPB and TCTA look similar and are shown in Supporting Information, Figure S7. The charged core molecule induces dipoles in environmental molecules, oriented to reduce Coulomb interactions with the charged core. This yields the largest component, the polarization itself, ΔV_0, that exceeds 2 eV. However, other components, referred to as depolarization, are negative and reduce the total polarization energy. First, induced dipoles of the nearest environmental molecules are oriented in nearly the same directions, leading to positive dipole−dipole interaction energy and, consequently, negative ΔV_{env}. Second, the field of the charged core molecule leads to an increase of the internal energy of environmental molecules and, consequently, negative ΔE_{env}. Finally, a charged core molecule experiences the field of induced dipoles of surrounding molecules, leading to the component, $\Delta\Delta E_0$. This component does not depend on the polarization radius and is not plotted in Figure 4a. For the sample molecules NPB and TCTA in this work, $\Delta\Delta E_0^{(-)}$ averaged over five core molecules is either zero or positive in contrast to the respective negative $\Delta\Delta E_0^{(+)}$, leading to an overall negative $\Delta\Delta E_0$. For C60, $\Delta\Delta E_0^{(\pm)}$ has the approximately same absolute value with the cation value being negative and the anion value being positive. We note that the depolarization energy components ΔV_{env} and ΔE_{env} and the contribution $\Delta\Delta E_0$ were not included in the conceptually similar method Quantum Patch,[7,25] leading to a significant overestimation of $P^{(+)}$ and $P^{(-)}$.

Figure 4b shows the cumulative sum of the polarization energy components starting from ΔV_0 for C60. The term $\Delta\Delta E_0$ is also included. The inset shows the percentage of each component (in absolute value). Thus, for C60, $|\Delta V_0|$, $|\Delta V_{env}|$, $|\Delta E_{env}|$, and $|\Delta\Delta E_0|$ contribute as 66.3%, 20.9%, 12.8%, and 0.0%. If we exclude $|\Delta\Delta E_0|$ from the consideration, these ratios will be almost the same for the three considered materials: 65.7 ± 0.3%, 21.0 ± 0.4%, and 13.3 ± 0.4% (see Supporting Information, Figure S8). Therefore, the 2:1 polarization to depolarization ratio may be a general rule for small organic molecules.

3.4. Cation vs Anion Polarization Energy. Figure 5 shows the total polarization energy of the cations and anions, $P^{(+)}/P^{(-)}$, of NPB and C60 as a function of the polarization radius, R. We note that this time the polarization energy is plotted separately for anions and cations; besides, the first component in eqs 7 and 10 is also included in $P^{(+)}$ and $P^{(-)}$, reflected in Figure 5 as negative polarization energy at polarization radii smaller than the distance to the first

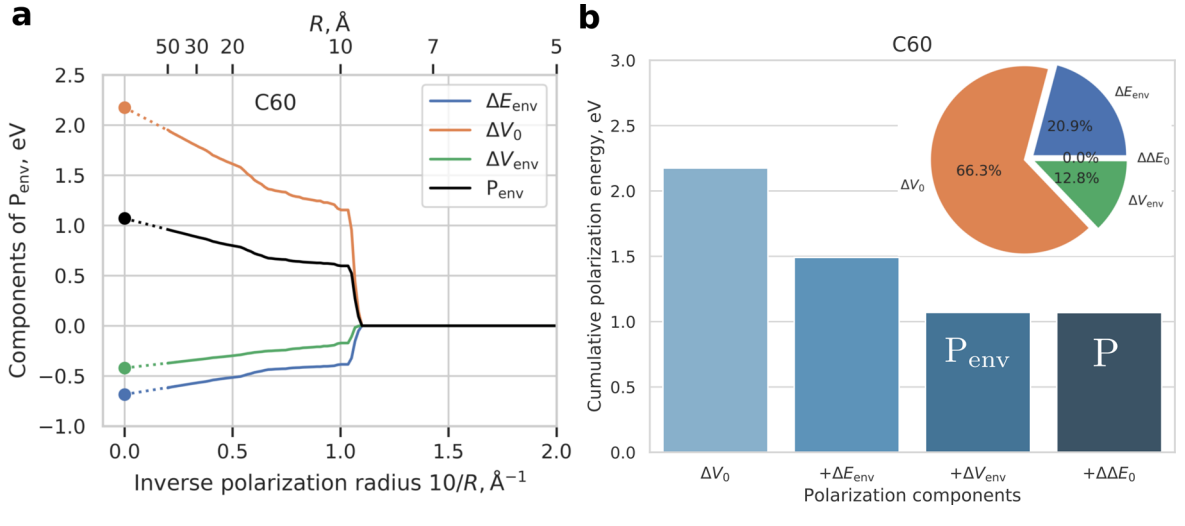

Figure 4. (a) Dependence of the averaged environmental polarization energy P_{env} (as introduced in eq 16) and its components on the polarization radius, R, for C60. (b) The cumulative sum of the polarization energy components starting from the polarization component ΔV_0. Adding so called depolarization components (ΔE_{env}, ΔV_{env}) and $\Delta\Delta E_0$ reduces the mean polarization energy from 2.18 eV down to 1.07 eV. Inset: the relation between *absolute* values of polarization energy components.

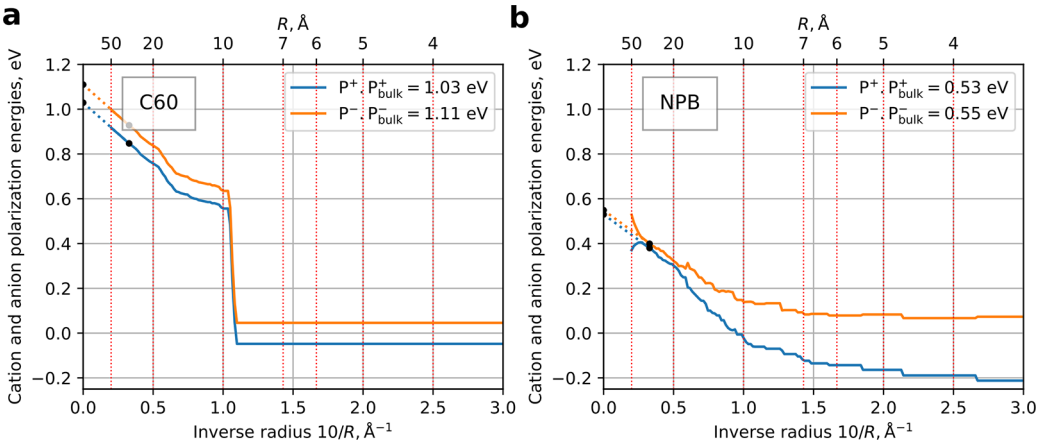

Figure 5. Determining the polarization energy of two materials: a) C60 and b) NPB. Solid lines show the explicitly computed polarization energy, separately for anions and cations, $P^{(+)}$ and $P^{(-)}$, as a function of the inverse polarization radius, $1/R$. The extrapolating lines, which slopes depend on ϵ_r, are shown with black dots. ϵ_r was determined by an average over cation and anion polarization energy for $R \in [20, 40]$ as explained in Section 3.2. Black points denote where the extrapolation begins (R = 30 Å) and ends ($R = \infty$). The starting point is chosen with a 20 Å offset from the explicit cutoff radius to avoid boundary effects which are well visible in NPB. Bulk polarization energy of cations and anions, $P^{(+)}_{bulk}$ and $P^{(-)}_{bulk}$, is defined as $P^{(+)}(R = \infty)$ and $P^{(-)}(R = \infty)$, respectively.

environmental molecule. The first point to notice is that the depolarization energy $\Delta\Delta E_0^{(+)}$ may be significantly different from zero (about −0.2 eV for a cation in NPB), which is observed as negative polarization energy even for an empty polarization sphere. In contrast, the polarization energy $\Delta\Delta E_0^{(-)}$ may be zero or even positive (about 0.07 eV for an anion in NPB). Besides, we can see that the polarization energy dependence on the polarization radius in the near field is not the same for anions and cations of NPB but is almost identical for C60 (but shifted by a constant offset due to the internal polarization energy). This can be explained by a high symmetry of C60, yielding similar charge distribution for both cations and anions. In contrast, NPB consists of various chemical groups, yielding different charge distributions. The exact source of this cation/anion "asymmetry" is out of this work scope; here, it is only essential that the method captures this difference.

Using the computed slope of $P(1/R)$ in Section 3.2, we have linearly extrapolated the polarization energy to an infinite polarization radius and obtained bulk polarization energies—see Figure 5. While the radius of the explicitly simulated system, R_{cut}, is 50 Å, the extrapolation line is drawn from point R = 30 Å to avoid boundary effects (i.e., the offset from the surface is 20 Å). Boundary effects are well visible in the plot for NPB, as they affect the polarization energy to be nonlinear in $1/R$. They are due to the transition from the polarizable medium to vacuum. Here, five core molecules were used; in contrast, Figure S9 of the SI demonstrates that a 10 Å offset is sufficient for one core molecule embedded into progressively larger polarization spheres (R_{cut}: 30 Å, 40 Å, 50 Å, and 60 Å).

3.5. Accuracy of the Method for the Polarization Energy. The accuracy of the computed polarization energies, $P^{(+)}/P^{(-)}$, is strongly related to the ability of the QM method to reproduce the true electron density. Considering that QM simulations are performed for every molecule within an explicit polarization shell (100−1000 molecules), the desirable QM method must be computationally efficient. Simultaneously, it must accurately reproduce the true electron density and the response to an external electric field. A thorough comparison of various DFT and wave function based methods[41] concerning their ability to reproduce the true electron density has shown that the generalized gradient approximations (GGA) of exchange correlation functionals, such as PBE[42] or BP86,[34] provide a mean normalized absolute error (MNAE) of the electron density descriptor of 1.12.[41] Importantly, hybrid GGA functionals are not much more accurate (e.g., for PBE0,[43] MNAE = 0.86) but much more "expensive", and some of them such as the Minnesota functional M06 2X[44] reproduce the electron density even worse than GGA: MNAE = 1.47.[41] Therefore, throughout this work, we use the BP86 functional as a reasonable compromise between the accuracy and the computational time. The basis set def2 SVPD is used because it is computationally efficient and is optimized for molecular response calculations (e.g., polarization response). It has only a 2% mean unsigned error compared to the basis set limit,[45] despite a small number of basis functions.

The computed polarization energy accuracy is also strongly related to the electron density response to the applied field and the leading term of this response, molecular polarizability. Benchmark simulations of small organic molecules that range in size from triatomics to 14 atoms[46] have shown that the root mean square relative error (RMSRE) of the computed polarizability using the PBE functional[42] is 6.45%. Assuming that the polarizability error propagates linearly to the polarization energy (having the order of 1 eV), we expect the mean error of the polarization energy of 64.5 meV, which is close to chemical accuracy, to be 1 kcal/mol ≈ 43 meV. However, this error is probably overestimated, as the test set contained small molecules, which polarizabilities are comparable to the absolute errors. According to another benchmark simulation, polarizabilities of a set of small molecules composed of elements from the first two rows of the main group computed with PBE has the root mean square deviation, RMSD = 0.41 Å^3,[47] which is around 0.5% of the absolute value of polarizabilities of organic molecules explored here (for NPB we computed: 115.4 Å^3; for C60: 82.9 Å^3—functional: BP86; basis set: def2 TZVPD). As our molecules have many more atoms than those in the mentioned benchmarks (e.g., NPB consists of 46 atoms other than the hydrogen), we have computed NPB and C60 polarizabilities using LDA functionals (S VWN, PWLDA, GGA) and PBE, BP86, and PLYP functionals, as well as a meta GGA (M06 L) functional. The

Table 3. Computed Polarization Energies $P^{(+/-)}$, Vacuum (vac), and Bulk IP/EA as well as the Approximations for Surface Ionization Potentials/Electron Affinities, EA_{surf}/IP_{surf}[a]

molecule	$P^{(+)}$	$P^{(-)}$	IP(vac)	EA(vac)	IP	EA	IP_{surf}	EA_{surf}
NPB	0.53	0.56	6.57	0.15	6.04	0.71	6.30	0.43
C60	1.03	1.11	7.78	2.79	6.75	3.90	7.27	3.35
TCTA	0.54	0.55	6.93	0.057	6.39	0.61	6.66	0.33

[a]See eqs 19 and 20. All values are in eV units.

NPB polarizability computed with these seven functionals falls into an interval between 115.0 $Å^3$ and 116.6 $Å^3$; C60 polarizability ranges from 82.5 to 83.2 $Å^3$. We may, thus, expect that the deviation of the computed polarizability using LDA/GGA functionals is around 1% for typical OLED molecules and that the error in the polarization energy may be as small as 0.01 eV.

In ref 48, it was shown that the choice of the exchange correlation functional influences the intermolecular transfer integral only slightly, but it is significantly changed by the fraction of the Hartree−Fock (HF) exchange in hybrid functionals. More specifically, the transfer integrals can vary by nearly a factor of 2 with respect to the fraction of nonlocal HF exchange incorporated in a standard hybrid functional.[48] To check if this is also the case for the polarization energy computed with our method, we did a benchmark calculation of the NPB molecule polarizability with meta GGA functionals incorporating different amounts of HF exchange (see Supporting Information, Section 10). The deviations of anion/cation polarization energy of one core molecule between BP86, M06 L[49] (0% HF exchange), M06[50] (27% HF exchange), and M06 2X[50] (54% HF exchange) do not exceed 0.1 eV for radii >20 Å. We consider this as a preliminary justification that the method is robust against both the choice of the exchange correlation functional and the amount of HF nonlocal exchange incorporated. In contrast to the magnitude of the intermolecular transfer integral that linearly increases with respect to the fraction of nonlocal HF exchange, we only see a slight increase of the *averaged* cation/anion polarization energy, while the individual anion/cation polarization energies show no clear trends. Moreover, the difference between different exchange correlation functionals that incorporate no HF exchange (BP86 and M06 L) is comparable to the difference between the hybrid functional of the same family with a different amount of HF exchange (M06 and M06 2X).

3.6. Determining the Ionization Potential and Electron Affinity of Embedded Molecules. We noted that the ionization potential and electron affinity of embedded molecules are IP = IP(vac) − $P^{(+)}$ and EA = EA(vac) + $P^{(-)}$. As discussed above, the combination of the computationally inexpensive BP86 functional and def2 SVPD basis set yields $P^{(\pm)}$ with almost chemical accuracy. To preserve a general accuracy of the method, vacuum IP/EA (EA(vac)/IP(vac)) have to be computed with the method that is as accurate as the method used for the polarization energy. However, the accuracy of IP/EA computation with GGA functionals is too low.[51] *Ab initio* methods, on the other hand, are prohibitively expensive for typical organic molecules used in OLEDs. Nevertheless, recent benchmark calculations[51−59] demonstrated that using a one step GW, i.e., G_0W_0 with the PBE0 hybrid functional[43] as an initial guess, provides accurate values of vertical IP/EA. For instance, the average error of 0.1 eV is reported[51] for G_0W_0: PBE0. In this work, we have used the eigenvalue self consistent scheme with PBE0[43] as a starting guess (ev GW:PBE0) and the def2 QZVP basis set as implemented in Turbomole.[40] Computed vacuum IP/EA are reported in Table 3. The bulk values obtained using formulas 1/2 as well as "surface" IP/EA values, IP_{surf}/EA_{surf}, are approximated as

$$IP_{surf} = IP(vac) - \frac{1}{2}P^{(+)} \tag{19}$$

$$EA_{surf} = EA(vac) + \frac{1}{2}P^{(-)} \tag{20}$$

and are reported in the same table. Accurate experimental data for C60 are available: experimental vertical EA[60] is 2.71 eV compared to our value of 2.79 eV; experimental IP[61] is 7.8 eV compared to our value of 7.78 eV. We expect that NPB and TCTA values computed in a vacuum are also close to their true values considering previous benchmarks. To the best of our knowledge, reported IP(vac)/EA(vac) for NPB and TCTA are the most accurate vacuum energies available in the literature for these molecules.

3.7. Comparison to Ultraviolet Photoelectron Spectroscopy/Inverse Photoemission Spectroscopy. While theoretical estimations outlined above suggest that the accuracy of the method is close to the chemical accuracy, experimental validation is more problematic. The reason is, strictly speaking, no available experimental technique can directly measure the mean ionization potential/electron affinity of the molecules embedded into the bulk material. Ultraviolet photoelectron spectroscopy (UPS)/inverse photoemission spectroscopy (IPES) are normally used for this purpose, but their interpretation is controversial. These techniques are primarily considered to be surface sensitive so that the measured response is received from one or several outermost molecular layers.[29] The polarization energy of these "semisurface" molecules is smaller than those embedded into an infinite (bulk) material because only half of the surrounding space is polarizable. It is sometimes assumed that the peaks on the UPS/IPES spectra correspond to vertical ionization energies, while onsets correspond to adiabatic ones.[62,63] According to a different point of view,[64] the onset of the UPS spectrum corresponds to the bulk IP, while the peak corresponds to the surface IP. The values reported in the literature for OLED materials are onsets of UPS/IPES spectra. Apart from being originated predominately from the surface of the unknown thickness and possibly containing reorganization energy contribution, onset energies are probably shifted toward the band gap due to additional stochastic contribution due to a measurement technique and other factors.[29,64] Finally, the resolution of UPS is typically up to 0.15 eV.[65,66] All those sources of uncertainty make IP/EA values reported in the literature[65,67−69] unreliable to a large extent. Therefore, we do not compare our results to the onset of UPS/IPES spectra. Instead, we directly superimpose our results on the combined

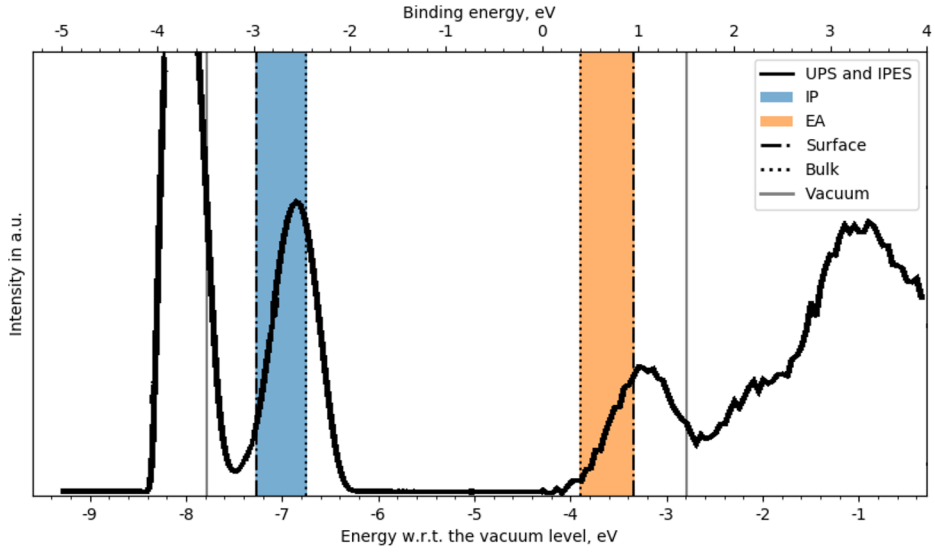

Figure 6. Comparison of experimental UPS and IPES spectra of C60 with computed values of IP/IP_{surf} and EA/EA_{surf}. The surface values are approximated using eqs 19 and 20. The first peak of the UPS (IPES) spectrum corresponding to IP(EA) falls between the surface and bulk IP(EA) suggesting that these techniques are sensitive to a surface layer, which has a thickness of a few molecular layers.

UPS/IPES spectra. Our method provides vertical IP/EA in bulk, and we have used a simple estimation for a surface IP/EA (formulas 19 and 20).

Figure 6 shows experimental UPS and IPES spectra of C60[66] together with vacuum, bulk, and surface IP/EA computed in this work. Both UPS and IPES peaks corresponding to IP/EA lie between our computed bulk and surface IP/EA values (shaded areas in the plot), suggesting that the UPS/IPES measured spectra are originated from a few outermost molecular layers. Figures S10 and S11 show IP and EA computed for TCTA and NPB together with experimental UPS and IPES spectra.

Several works reported direct comparison of measured UPS/IPES spectra to single particle energy levels computed at various levels of the theory, e.g., semiempirical Hartree−Fock approaches.[66,70] In those works, single particle energy levels were computed in a vacuum. To fit experimental spectra, these were spread and shifted toward lower energies (in the case of UPS) and finally compressed by a factor of 1.3. Unlike our method, those approaches do not allow for quantitative prediction of the bulk IP/EA.

4. CONCLUSION

In conclusion, an accurate method for amorphous organic semiconductors is proposed that enables calculation of the ionization potential, electron affinity, polarization energies of embedded molecules, and dielectric permittivity of the material. Based on a quantum embedding (QM/QM) scheme, our method features numerical efficiency and the accuracy of QM methods. This is reached by treating intramolecular interactions in the whole explicitly simulated material at the QM level (DFT and GW). In contrast, intermolecular interactions are approximated by classical interactions between point charges, derived from QM simulations. Based on the accuracy of the constituent methods, we estimate the accuracy of our method to be less than 0.1 eV for both polarization energy and vacuum IP/EA. The accuracy can be systematically improved if more accurate QM methods will become available for relevant molecules. High accuracy is achieved due to a well balanced selection of the level of the theory in QM simulation: the GW method and a large basis set are used to compute IP/EA of a core molecule. In contrast, GGA DFT and a computationally efficient basis set are used to compute polarization energies.

Natural separation of the total energy of the material into intramolecular and intermolecular contributions allowed us to identify and quantify four sources of the polarization energy—this is the first step to control the polarization by a molecular design. We have established that the polarization/depolarization ratio is about 2:1 for all materials simulated in this work.

We have applied the method to three prototypical OLED materials, C60, NPB, and TCTA, and found that the extracted dielectric permittivities agree with reported experimental data proving a correct "asymptotic" behavior of the method. Direct comparison of computed IP/EA of embedded C60 molecules to experimental UPS/IPES spectra showed that respective peaks at UPS/IPES are between our calculated values for bulk and surface IP/EA, since UPS/IPES are surface sensitive techniques. We hope that our results will improve the virtual screening of amorphous organic semiconductors with the desired IP/EA, polarization energies, and relative dielectric permittivities.

AUTHOR INFORMATION

Corresponding Author

Artem Fediai − *Institute of Nanotechnology, Karlsruhe Institute of Technology, 76344 Karlsruhe, Germany;* orcid.org/0000 0002 4156 115X; Email: artem.fediai@kit.edu

Authors

Jonas Armleder − *Institute of Nanotechnology, Karlsruhe Institute of Technology, 76344 Karlsruhe, Germany*

Timo Strunk − *Nanomatch GmbH, 76185 Karlsruhe, Germany*

Franz Symalla − *Nanomatch GmbH, 76185 Karlsruhe, Germany*

Pascal Friederich − *Institute of Theoretical Informatics, Karlsruhe Institute of Technology, 76344 Karlsruhe, Germany; Nanomatch GmbH, 76185 Karlsruhe, Germany;* orcid.org/0000 0003 4465 1465

Jorge Enrique Olivares Peña − *Institute of Nanotechnology, Karlsruhe Institute of Technology, 76344 Karlsruhe, Germany*

Tobias Neumann − *Nanomatch GmbH, 76185 Karlsruhe, Germany*

Wolfgang Wenzel − *Institute of Nanotechnology, Karlsruhe Institute of Technology, 76344 Karlsruhe, Germany*

Notes

The author declare the following competing financial interest(s): W.W. holds shares of a KIT spinoff, Nanomatch GmbH, which markets software developed by KIT. The other authors declare no competing interests.

■ ACKNOWLEDGMENTS

W.W. acknowledges funding from the Deutsche Forschungs gemeinschaft (DFG, German Research Foundation) under Germany Excellence Strategy via the Excellence Cluster 3D Matter Made to Order (EXC 2082/1 390761711) and from the DFG through the Research Training Group 2450 "Tailored Scale Bridging Approaches to Computational Nanoscience". J.E.O.P. acknowledge the grants DFG: FE 1776/2 1 and DFG: WE 1863/34 1. This work was performed on the super computer ForHLR II funded by the Ministry of Science, Research and the Arts Baden Württemberg and by the Federal Ministry of Education and Research.

■ REFERENCES

(1) Geffroy, B.; le Roy, P.; Prat, C. Organic light emitting diode (OLED) technology: materials, devices and display technologies. *Polym. Int.* **2006**, *55*, 572−582.

(2) Mei, J.; Diao, Y.; Appleton, A. L.; Fang, L.; Bao, Z. Integrated Materials Design of Organic Semiconductors for Field Effect Transistors. *J. Am. Chem. Soc.* **2013**, *135*, 6724−6746.

(3) Ameri, T.; Dennler, G.; Lungenschmied, C.; Brabec, C. J. Organic tandem solar cells: A review. *Energy Environ. Sci.* **2009**, *2*, 347−363.

(4) Friederich, P.; Fediai, A.; Kaiser, S.; Konrad, M.; Jung, N.; Wenzel, W. Toward Design of Novel Materials for Organic Electronics. *Adv. Mater.* **2019**, *31*, 1808256.

(5) D'Avino, G.; Muccioli, L.; Castet, F.; Poelking, C.; Andrienko, D.; Soos, Z. G.; Cornil, J.; Beljonne, D. Electrostatic phenomena in organic semiconductors: fundamentals and implications for photo voltaics. *J. Phys.: Condens. Matter* **2016**, *28*, 433002.

(6) Li, J.; Duchemin, I.; Roscioni, O. M.; Friederich, P.; Anderson, M.; Da Como, E.; Kociok Köhn, G.; Wenzel, W.; Zannoni, C.; Beljonne, D.; Blase, X.; D'Avino, G. Host dependence of the electron affinity of molecular dopants. *Mater. Horiz.* **2019**, *6*, 107−114.

(7) Friederich, P.; Symalla, F.; Meded, V.; Neumann, T.; Wenzel, W. Ab Initio Treatment of Disorder Effects in Amorphous Organic Materials: Toward Parameter Free Materials Simulation. *J. Chem. Theory Comput.* **2014**, *10*, 3720−3725.

(8) Duhm, S.; Heimel, G.; Salzmann, I.; Glowatzki, H.; Johnson, R. L.; Vollmer, A.; Rabe, J. P.; Koch, N. Orientation dependent ionization energies and interface dipoles in ordered molecular assemblies. *Nat. Mater.* **2008**, *7*, 326−332.

(9) Chen, W.; Huang, H.; Chen, S.; Huang, Y. L.; Gao, X. Y.; Wee, A. T. S. Molecular Orientation Dependent Ionization Potential of Organic Thin Films. *Chem. Mater.* **2008**, *20*, 7017−7021.

(10) Fediai, A.; Symalla, F.; Friederich, P.; Wenzel, W. Disorder compensation controls doping efficiency in organic semiconductors. *Nat. Commun.* **2019**, *10*, 4547.

(11) Fediai, A.; Emering, A.; Symalla, F.; Wenzel, W. Disorder driven doping activation in organic semiconductors. *Phys. Chem. Chem. Phys.* **2020**, *22*, 10256−10264.

(12) Symalla, F.; Fediai, A.; Armleder, J.; Kaiser, S.; Strunk, T.; Neumann, T.; Wenzel, W. 43−3: Ab initio Simulation of Doped Injection Layers. *Dig. Tech. Pap. Soc. Inf. Disp. Int. Symp.* **2020**, *51*, 630−633.

(13) Ren, P.; Ponder, J. W. Consistent treatment of inter and intramolecular polarization in molecular mechanics calculations. *J. Comput. Chem.* **2002**, *23*, 1497−1506.

(14) Ponder, J. W.; Wu, C.; Ren, P.; Pande, V. S.; Chodera, J. D.; Schnieders, M. J.; Haque, I.; Mobley, D. L.; Lambrecht, D. S.; DiStasio, R. A.; Head Gordon, M.; Clark, G. N. I.; Johnson, M. E.; Head Gordon, T. Current Status of the AMOEBA Polarizable Force Field. *J. Phys. Chem. B* **2010**, *114*, 2549−2564.

(15) Fuchs, A.; Steinbrecher, T.; Mommer, M. S.; Nagata, Y.; Elstner, M.; Lennartz, C. Molecular origin of differences in hole and electron mobility in amorphous Alq3—a multiscale simulation study. *Phys. Chem. Chem. Phys.* **2012**, *14*, 4259−4270.

(16) Poelking, C.; Andrienko, D. Long Range Embedding of Molecular Ions and Excitations in a Polarizable Molecular Environ ment. *J. Chem. Theory Comput.* **2016**, *12*, 4516−4523.

(17) Åqvist, J.; Warshel, A. Simulation of enzyme reactions using valence bond force fields and other hybrid quantum/classical approaches. *Chem. Rev.* **1993**, *93*, 2523−2544.

(18) Difley, S.; Wang, L. P.; Yeganeh, S.; Yost, S. R.; Voorhis, T. V. Electronic Properties of Disordered Organic Semiconductors via QM/MM Simulations. *Acc. Chem. Res.* **2010**, *43*, 995−1004.

(19) Kwiatkowski, J. J.; Nelson, J.; Li, H.; Bredas, J. L.; Wenzel, W.; Lennartz, C. Simulating charge transport in tris(8 hydroxyquinoline) aluminium (Alq3). *Phys. Chem. Chem. Phys.* **2008**, *10*, 1852−1858.

(20) Li, J.; D'Avino, G.; Duchemin, I.; Beljonne, D.; Blase, X. Accurate description of charged excitations in molecular solids from embedded many body perturbation theory. *Phys. Rev. B: Condens. Matter Mater. Phys.* **2018**, *97*, 035108.

(21) Norton, J. E.; Brédas, J. L. Polarization Energies in Oligoacene Semiconductor Crystals. *J. Am. Chem. Soc.* **2008**, *130*, 12377−12384.

(22) Castet, F.; Aurel, P.; Fritsch, A.; Ducasse, L.; Liotard, D.; Linares, M.; Cornil, J.; Beljonne, D. Electronic polarization effects on charge carriers in anthracene: A valence bond study. *Phys. Rev. B: Condens. Matter Mater. Phys.* **2008**, *77*, 115210.

(23) Castet, F.; Ducasse, L.; Fritsch, A. From organic super conductors to DNA: Fragment orbital based model. *Int. J. Quantum Chem.* **2006**, *106*, 734−746.

(24) Ratcliff, L. E.; Danilov, D.; Wenzel, W.; Beljonne, D. Toward Fast and Accurate Evaluation of Charge On Site Energies and Transfer Integrals in Supramolecular Architectures Using Linear Constrained Density Functional Theory (CDFT) Based Methods. *J. Chem. Theory Comput.* **2015**, *11*, 2077−2086.

(25) Friederich, P.; Meded, V.; Symalla, F.; Elstner, M.; Wenzel, W. QM/QM Approach to Model Energy Disorder in Amorphous Organic Semiconductors. *J. Chem. Theory Comput.* **2015**, *11*, 560−567.

(26) Senatore, G.; Subbaswamy, K. R. Density dependence of the dielectric constant of rare gas crystals. *Phys. Rev. B: Condens. Matter Mater. Phys.* **1986**, *34*, 5754−5757.

(27) Johnson, M. D.; Subbaswamy, K. R.; Senatore, G. Hyper polarizabilities of alkali halide crystals using the local density approximation. *Phys. Rev. B: Condens. Matter Mater. Phys.* **1987**, *36*, 9202−9211.
(28) Cortona, P. Self consistently determined properties of solids without band structure calculations. *Phys. Rev. B: Condens. Matter Mater. Phys.* **1991**, *44*, 8454−8458.
(29) Gaul, C.; Hutsch, S.; Schwarze, M.; Schellhammer, K. S.; Bussolotti, F.; Kera, S.; Cuniberti, G.; Leo, K.; Ortmann, F. Insight into doping efficiency of organic semiconductors from the analysis of the density of states in n doped C60 and ZnPc. *Nat. Mater.* **2018**, *17*, 439−444.
(30) Nell, B.; Ortstein, K.; Boltalina, O. V.; Vandewal, K. Influence of Dopant−Host Energy Level Offset on Thermoelectric Properties of Doped Organic Semiconductors. *J. Phys. Chem. C* **2018**, *122*, 11730−11735.
(31) Pope, M. *Electronic processes in organic crystals and polymers*, 2nd ed. ed.; Monographs on the physics and chemistry of materials #56; Oxford University Press: New York, 1999.
(32) Neumann, T.; Danilov, D.; Lennartz, C.; Wenzel, W. Modeling disordered morphologies in organic semiconductors. *J. Comput. Chem.* **2013**, *34*, 2716−2725.
(33) Kim, K.; Jordan, K. D. Comparison of Density Functional and MP2 Calculations on the Water Monomer and Dimer. *J. Phys. Chem.* **1994**, *98*, 10089−10094.
(34) Becke, A. D. Density functional exchange energy approxima tion with correct asymptotic behavior. *Phys. Rev. A: At., Mol., Opt. Phys.* **1988**, *38*, 3098−3100.
(35) Eklund, P. C.; Rao, A. M.; Wang, Y.; Zhou, P.; Wang, K. A.; Holden, J. M.; Dresselhaus, M. S.; Dresselhaus, G. Optical properties of C60 and C70 based solid films. *Thin Solid Films* **1995**, *257*, 211−232.
(36) Shin, H.; Lee, J. H.; Moon, C. K.; Huh, J. S.; Sim, B.; Kim, J. J. Sky Blue Phosphorescent OLEDs with 34.1% External Quantum Efficiency Using a Low Refractive Index Electron Transporting Layer. *Adv. Mater.* **2016**, *28*, 4920−4925.
(37) Hermann, S.; Gordan, O. D.; Friedrich, M.; Zahn, D. R. T. Optical properties of multilayered Alq3/a NPD structures inves tigated with spectroscopic ellipsometry. *Phys. Status Solidi C* **2005**, *2*, 4037−4042.
(38) de Vries, X.; Coehoorn, R. Vibrational mode contribution to the dielectric permittivity of disordered small molecule organic semiconductors. *Phys. Rev. Mater.* **2020**, *4*, 085602.
(39) Jackson, J. D. *Classical electrodynamics*; 2nd ed.; Wiley: New York, NY, 1975.
(40) Balasubramani, S. G.; Chen, G. P.; Coriani, S.; Diedenhofen, M.; Frank, M. S.; Franzke, Y. J.; Furche, F.; Grotjahn, R.; Harding, M. E.; Hättig, C.; Hellweg, A.; Helmich Paris, B.; Holzer, C.; Huniar, U.; Kaupp, M.; Marefat Khah, A.; Karbalaei Khani, S.; Müller, T.; Mack, F.; Nguyen, B. D.; Parker, S. M.; Perlt, E.; Rappoport, D.; Reiter, K.; Roy, S.; Rückert, M.; Schmitz, G.; Sierka, M.; Tapavicza, E.; Tew, D. P.; van Wüllen, C.; Voora, V. K.; Weigend, F.; Wodyński, A.; Yu, J. M. TURBOMOLE: Modular program suite for ab initio quantum chemical and condensed matter simulations. *J. Chem. Phys.* **2020**, *152*, 184107.
(41) Medvedev, M. G.; Bushmarinov, I. S.; Sun, J.; Perdew, J. P.; Lyssenko, K. A. Density functional theory is straying from the path toward the exact functional. *Science* **2017**, *355*, 49−52.
(42) Perdew, J. P.; Burke, K.; Ernzerhof, M. Generalized Gradient Approximation Made Simple. *Phys. Rev. Lett.* **1996**, *77*, 3865−3868.
(43) Adamo, C.; Barone, V. Toward reliable density functional methods without adjustable parameters: The PBE0 model. *J. Chem. Phys.* **1999**, *110*, 6158−6170.
(44) Zhao, Y.; Truhlar, D. G. Exploring the Limit of Accuracy of the Global Hybrid Meta Density Functional for Main Group Thermo chemistry, Kinetics, and Noncovalent Interactions. *J. Chem. Theory Comput.* **2008**, *4*, 1849−1868.
(45) Rappoport, D.; Furche, F. Property optimized Gaussian basis sets for molecular response calculations. *J. Chem. Phys.* **2010**, *133*, 134105.
(46) Wu, T.; Kalugina, Y. N.; Thakkar, A. J. Choosing a density functional for static molecular polarizabilities. *Chem. Phys. Lett.* **2015**, *635*, 257−261.
(47) Hickey, A. L.; Rowley, C. N. Benchmarking Quantum Chemical Methods for the Calculation of Molecular Dipole Moments and Polarizabilities. *J. Phys. Chem. A* **2014**, *118*, 3678−3687.
(48) Sutton, C.; Sears, J. S.; Coropceanu, V.; Brédas, J. L. Understanding the Density Functional Dependence of DFT Calculated Electronic Couplings in Organic Semiconductors. *J. Phys. Chem. Lett.* **2013**, *4*, 919−924.
(49) Zhao, Y.; Truhlar, D. G. A new local density functional for main group thermochemistry, transition metal bonding, thermochem ical kinetics, and noncovalent interactions. *J. Chem. Phys.* **2006**, *125*, 194101.
(50) Zhao, Y.; Truhlar, D. G. The M06 suite of density functionals for main group thermochemistry, thermochemical kinetics, non covalent interactions, excited states, and transition elements: two new functionals and systematic testing of four M06 class functionals and 12 other functionals. *Theor. Chem. Acc.* **2008**, *120*, 215−241.
(51) Wilhelm, J.; Del Ben, M.; Hutter, J. GW in the Gaussian and Plane Waves Scheme with Application to Linear Acenes. *J. Chem. Theory Comput.* **2016**, *12*, 3623−3635.
(52) Ren, X.; Rinke, P.; Blum, V.; Wieferink, J.; Tkatchenko, A.; Sanfilippo, A.; Reuter, K.; Scheffler, M. Resolution of identity approach to Hartree−Fock, hybrid density functionals, RPA, MP2 andGWwith numeric atom centered orbital basis functions. *New J. Phys.* **2012**, *14*, 053020.
(53) Bruneval, F.; Marques, M. A. L. Benchmarking the Starting Points of the GW Approximation for Molecules. *J. Chem. Theory Comput.* **2013**, *9*, 324−329.
(54) Jacquemin, D.; Duchemin, I.; Blase, X. Benchmarking the Bethe−Salpeter Formalism on a Standard Organic Molecular Set. *J. Chem. Theory Comput.* **2015**, *11*, 3290−3304.
(55) Körbel, S.; Boulanger, P.; Duchemin, I.; Blase, X.; Marques, M. A. L.; Botti, S. Benchmark Many Body GW and Bethe−Salpeter Calculations for Small Transition Metal Molecules. *J. Chem. Theory Comput.* **2014**, *10*, 3934−3943.
(56) Govoni, M.; Galli, G. Large Scale GW Calculations. *J. Chem. Theory Comput.* **2015**, *11*, 2680−2696.
(57) Marom, N.; Caruso, F.; Ren, X.; Hofmann, O. T.; Körzdörfer, T.; Chelikowsky, J. R.; Rubio, A.; Scheffler, M.; Rinke, P. Benchmark of *GW* methods for azabenzenes. *Phys. Rev. B: Condens. Matter Mater. Phys.* **2012**, *86*, 245127.
(58) Atalla, V.; Yoon, M.; Caruso, F.; Rinke, P.; Scheffler, M. Hybrid density functional theory meets quasiparticle calculations: A consistent electronic structure approach. *Phys. Rev. B: Condens. Matter Mater. Phys.* **2013**, *88*, 165122.
(59) Marom, N.; Ren, X.; Moussa, J. E.; Chelikowsky, J. R.; Kronik, L. Electronic structure of copper phthalocyanine from G_0W_0 calculations. *Phys. Rev. B: Condens. Matter Mater. Phys.* **2011**, *84*, 195143.
(60) Palpant, B.; Negishi, Y.; Sanekata, M.; Miyajima, K.; Nagao, S.; Judai, K.; Rayner, D. M.; Simard, B.; Hackett, P. A.; Nakajima, A.; Kaya, K. Electronic and geometric properties of exohedral sodium and gold fullerenes. *J. Chem. Phys.* **2001**, *114*, 8459−8466.
(61) Muigg, D.; Scheier, P.; Becker, K.; Märk, T. D. Measured appearance energies of fragment ions produced by electron impact on. *J. Phys. B: At., Mol. Opt. Phys.* **1996**, *29*, 5193−5198.
(62) Eland, J. H. D. *Photoelectron spectroscopy: an introduction to ultraviolet photoelectron spectroscopy in the gas phase*, 2nd ed.; Butterworths: London [u.a.], 1984; LiteraturangabenIMD Felder maschinell generiert (GBV), DOI: 10.1016/C2013 0 01044 4.
(63) Turner, D. In *Ionization Potentials*; Gold, V., Ed.; Advances in Physical Organic Chemistry; Academic Press: 1966; Vol. *4*, pp 31 − 71, DOI: 10.1016/S0065 3160(08)60352 4.

(64) Sato, N.; Seki, K.; Inokuchi, H. Polarization energies of organic solids determined by ultraviolet photoelectron spectroscopy. *J. Chem. Soc., Faraday Trans. 2* **1981**, *77*, 1621−1633.
(65) Zhang, F.; Kahn, A. Investigation of the High Electron Affinity Molecular Dopant F6 TCNNQ for Hole Transport Materials. *Adv. Funct. Mater.* **2018**, *28*, 1703780.
(66) Hill, I.; Kahn, A.; Cornil, J.; dos Santos, D.; Brédas, J. Occupied and unoccupied electronic levels in organic pi conjugated molecules: comparison between experiment and theory. *Chem. Phys. Lett.* **2000**, *317*, 444−450.
(67) Hill, I. G.; Kahn, A. Organic semiconductor heterointerfaces containing bathocuproine. *J. Appl. Phys.* **1999**, *86*, 4515−4519.
(68) White, R. T.; Thibau, E. S.; Lu, Z. H. Interface Structure of MoO3 on Organic Semiconductors. *Sci. Rep.* **2016**, *6*, 21109.
(69) Guan, Z. L.; Bok Kim, J.; Loo, Y. L.; Kahn, A. Electronic structure of the poly(3 hexylthiophene):indene C_{60} bisadduct bulk heterojunction. *J. Appl. Phys.* **2011**, *110*, 043719.
(70) Cornil, J.; Vanderdonckt, S.; Lazzaroni, R.; dos Santos, D. A.; Thys, G.; Geise, H. J.; Yu, L. M.; Szablewski, M.; Bloor, D.; Lögdlund, M.; Salaneck, W. R.; Gruhn, N. E.; Lichtenberger, D. L.; Lee, P. A.; Armstrong, N. R.; Brédas, J. L. Valence Electronic Structure of pi Conjugated Materials: Simulation of the Ultraviolet Photoelectron Spectra with Semiempirical Hartree Approaches. *Chem. Mater.* **1999**, *11*, 2436−2443.